RSC Advances

PAPER

View Article Online
View Journal | View Issue

Cite this: *RSC Adv.*, 2020, **10**, 26006

Design, synthesis, biological evaluation and molecular docking study of novel pyridoxine–triazoles as anti-Alzheimer's agents†

Tiyas Pal,[a] Saipriyanka Bhimaneni,[b] Abha Sharma *[a] and S. J. S. Flora *[b]

Received 4th June 2020
Accepted 3rd July 2020

DOI: 10.1039/d0ra04942e

rsc.li/rsc-advances

A series of multi-target natural product-pyridoxine based derivatives were designed, synthesized, characterized and evaluated as anti-Alzheimer agents. *In vitro* testing revealed the multi-functional properties of compounds such as inhibition of acetylcholinesterase (AChE), antioxidant and metal chelation. Among the series, **5i** derivative was found most potent AChE inhibitor, possess antioxidant potential and chelating metal ions. Further binding interaction of **5i** with AChE was studied using molecular docking, showed interaction with both PAS and CAS site of AChE. *In silico* predictions were also performed to predict toxicity and ADME properties of the molecule **5i** and found within drug likeness range. Therefore, **5i** could be a promising multi-functional compound that can be used for further development of novel drug for Alzheimer disease.

1 Introduction

Alzheimer's disease (AD) is the most challenging neurodegenerative disease affecting mostly the population above 65 years of age. The perplexing nature of the disease makes it all more difficult for its ministration. More than 50 million are suffering globally and the number is likely to get hiked up to 150 million by the year 2050.[1] The multifaceted nature of the disease with several interconnected etiologies led to the idea of developing multi-target directed ligands (MTDLs). MTDLs in the field of neurodegenerative diseases is now a very significant area of research developed by academia and industry.[2,3] The design of MTDL comprises two or more pharmacophore moieties which are responsible for targeting multiple targets which are accountable for the pathogenesis of the disease. Therefore, MTDLs are single molecules with multiple functions which are strategically designed to serve the purpose of developing potential new chemical entities that can be used against AD.

The currently available Food and Drug Administration (FDA) approved drugs mainly focus on the cholinergic hypothesis, as one of the most excavated areas to slow down the progression of AD. Cholinergic hypothesis, amyloid-β cascade hypothesis, metal dyshomeostasis, tau hypothesis and oxidative stress hypothesis are some of the identified etiologies responsible for this disease. Damage to cholinergic neurons lead to cognitive decline which showed the way to develop acetylcholinesterase (AChE) inhibitors providing symptomatic relief to the AD patients. However, this age related disease poses a problem of uncontrollable bio-burden of metal ions in the brain. This metal dyshomeostasis in turn induces oxidative stress and formation of amyloid-β (Aβ) plaques. Due to this interconnection of etiologies, classical metal chelator cannot do any benefit to this existing problem of the disease. Therefore MTDLs is needed in this juncture. Increase in biometals amplifies reactive oxygen species (ROS) which includes augmentation of lipid peroxidation, protein oxidation, nitration and glycol oxidation. Oxidative stress aggravates the pathophysiological conditions of neuronal damage.[4] A molecule having additional anti-oxidant potency along with AChE inhibitory potential and metal chelating ability can be developed as a potential anti-AD agent. Studies have stated that peripheral anionic site (PAS) binding of AChE may promote Aβ aggregation. For PAS binding, aromatic rings with pi–pi stacking are recommended as derived from the docking studies with donepezil.[5]

In light of the concepts mentioned above, and to focus on our efforts to develop a new class of anti-Alzheimer's agents as MTDLs, we focused on the synthesis of pyridoxine based 1,2,3-triazoles and its biological evaluation. We assessed the synthesized compounds for AChE inhibition, antioxidant potency, metal chelation ability using *in vitro* assays as screening methods. We predicted various pharmacokinetic properties and toxicity of the best compound of the series using *in silico* tools.

2 Results and discussion

2.1 Design

Nitrogen heterocycles have long been of medical interest[6–8] while, triazoles falling under the category of nitrogen

[a]Department of Medicinal Chemistry, National Institute of Pharmaceutical Education and Research, Raebareli, India. E-mail: abha.sharma@niperraebareli.edu.in

[b]Department of Regulatory Toxicology, National Institute of Pharmaceutical Education and Research, Raebareli, India. E-mail: sjsflora@hotmail.com

† Electronic supplementary information (ESI) available: Spectra data. See DOI: 10.1039/d0ra04942e

heterocycles have been the moiety of interest. Numerous molecules with triazole moiety have been reported. In this regard, Rastegari *et al.* reported 1,2,3-triazole chromenone carboxamide derivatives as AChE inhibitors.[9] Jalili-Baleh *et al.* developed 3-phenylcoumarin lipoic acid based triazole derivatives as anti-Alzheimer's agents.[10] Fig. 1 provides a summary of few triazole and pyridoxine containing molecules reported recently as potential anti-Alzheimer's agents.[9–15]

Pyridoxine is known to reduce homocysteine levels in Alzheimer's patients. Homocysteine is derived from amino acid methionine and is a non-protein homologue of cysteine. The directly attached hydroxyl group to the pyridine nucleus might be playing a role in chelation of metal and also for the antioxidant properties. Pyridoxine has successfully completed the phase 3 clinical trials as a vitamin which can reduce homocysteine levels in AD affected patients. The circulating high level of homocysteine in AD is responsible for deposition of amyloid β plaques.[16,17] Pyridoxine–resveratrol have been reported as only pyridoxine based compounds against AD. However, pyridoxine based triazoles have not been reported and therefore, herein we report this new class of compounds.

Taking into the consideration the multifaceted nature of the disease, we designed pyridoxine based 1,2,3-triazoles as an MTDL which might be an effective agents against AD. We have designed our target molecules containing both the pyridoxine and triazole moiety as a new class of MTDL using linking approach. Fig. 2 provides the possible hypothesis behind the designing of our target molecules.

2.2 Chemistry

We synthesized pyridoxine based triazoles derivatives (Scheme 1). The target molecules were synthesized *via* four step reaction scheme using pyridoxine hydrochloride (**1**) as starting material. In the first step, commercially available pyridoxine hydrochloride (**1**) was protected at the 3- and 4-hydroxy groups using *p*-toluenesulfonic acid monohydrate and dry acetone in the

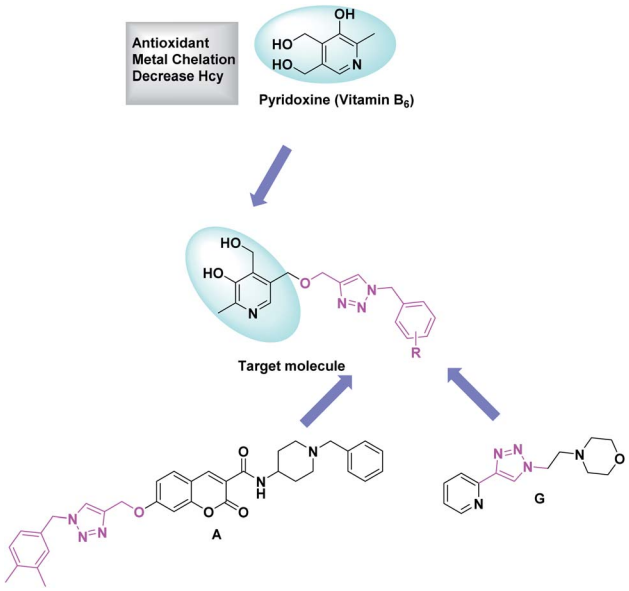

Fig. 2 Design of target molecules chemistry.

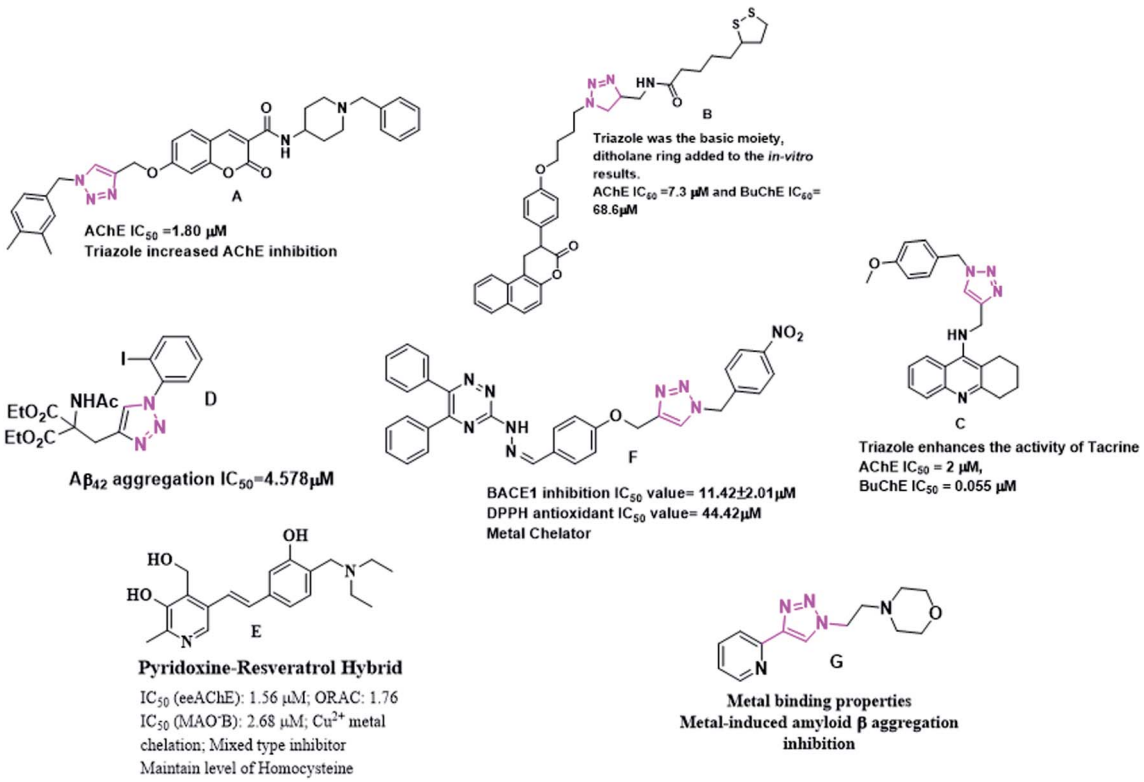

Fig. 1 Triazole and pyridoxine containing molecules as anti-Alzheimer's agents.

presence of 2,2-dimethoxypropane under argon atmosphere. Then compound **2** was treated with propargyl bromide using NaH as base and dry THF as solvent under argon atmosphere to give compound **3**. In the next step, various substituted benzyl azides were generated *in situ* from benzyl bromides followed by synthesis of triazole moiety after addition of compound **3** using the classical CuAAC, generating compounds **4(a–q)**. Finally, target compounds **5(a–q)** were obtained through deprotection of the isopropylidene group.

2.3 *In vitro* assay of AChE inhibition

The *in vitro* activity of the new synthesized molecules was done using AChE from electric eel (EeAChE) following Ellman's method.[25] All the molecules were tested for their ability to inhibit AChE activity, keeping donepezil as the reference compound. The IC_{50} values of the molecules are summarized in Table 1. AChE inhibition remains a very critical end point in slowing down the progression of the disease, and thus we selected to determine the ability of our compounds to inhibit the aforesaid enzyme.

2.3.1 Structure activity relationship. Our target molecule contains triazole and pyridoxine moieties incorporated into it. Before starting our investigation on our library of compounds **5(a–q)**, we sought to find out the inhibitory activity of pyridoxine on AChE and observed it to be inactive against the enzyme; these results correlated well with the studies of Drtinova *et al.*[18] We also sought to find out the effect of triazole moiety and substitution on the aromatic ring on enzymatic activity.

The unsubstituted **5a** did not show much inhibition even at the highest concentration (10 mM), thus can be considered inactive towards the enzyme. With the substitution of methyl group at the *para* position (**5b**) it however, showed inhibitory activity as compared to **5a**. By changing the position of methyl group from *para* to *meta* (**5c**) and *ortho* (**5d**) position, a marked change was noted. A *meta* substitution of the electron donating group (EDG) offered a better inhibitory activity almost twice potent as compared to **5b**, while the *ortho* alkyl substitution proved even better. Substitution of methoxy group at the 3rd position (**5e**) and at 3rd and 5th position of the aromatic ring (**5f**) had no inhibitory activity, however, methyl substitution proved better than these. A double methoxy substitution was found more efficacious compared with its single substitution.

We further explored by trying different halides as substituents and their effect on the inhibition on the enzyme. We also synthesized F, Cl and Br derivatives at different position. Halogens are supposed to have +R effect on the aromatic ring, despite of their position. When the effect of halogen is observed at the *para* position, fluoro substituent (**5g**) showed lesser efficacy compared to –Cl (**5j**) and –Br (**5m**) derivatives. However, we did not find a uniform trend in activity as we moved down the periodic table. Chloro substitution at the *para* position was more potent in comparison to bromo substitution. However, *meta* substitution of halogens showed much better results as compared to the *para* substitution. Change in position from *para* to *meta* did not prove successful in improving potency in chloro substitution (**5k**), as there was no such change in the IC_{50} value. Bromine at the 3rd position of the aromatic ring (**5n**) was more active in comparison to the fluoro substitution (**5h**). We even tried to find out the effect of substitution when two positions on the aromatic ring are occupied with the halogen atoms. We thus included fluorine in 3rd and 5th position (**5i**) and in

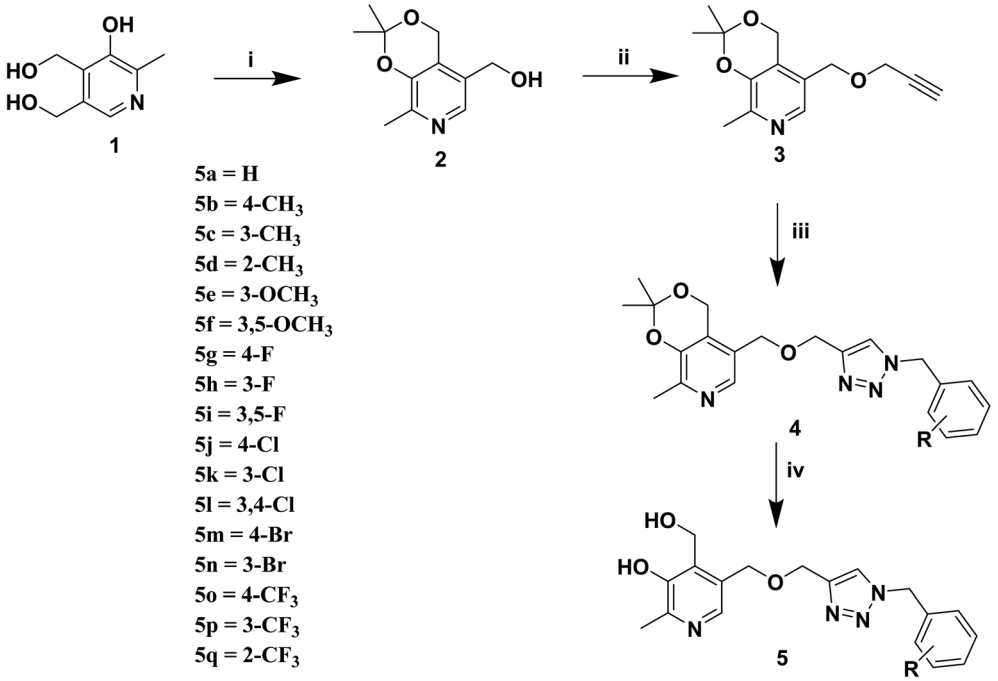

Scheme 1 Reagents and conditions-(i) 2,2-dimethoxypropane, *p*-toluenesulfonic acid monohydrate, anhydrous acetone, under argon atmosphere 20 h, rt (ii) NaH, propargyl bromide, dry THF, reflux under argon atmosphere, 4 h (iii) benzyl bromide, NaN_3, triethylamine, $CuSO_4 \cdot 5H_2O$ (10 mol%), ascorbic acid (25 mol%), *t*-BuOH : H_2O (1 : 1), reflux for 6–12 h (iv) THF, 10% conc. sulphuric acid, 70 °C, 6–12 h.

Table 1 Results of AChE inhibition and anti-oxidant values

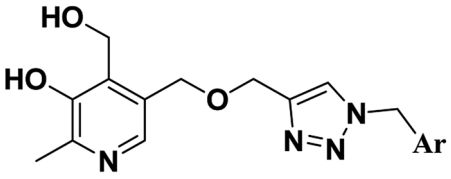

5

Compound	Ar	EeAChE IC_{50} ± SEM[a] (mM)		ORAC index ± SEM[b]	
5a	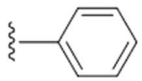	>10		1.0564	±0.3604
5b	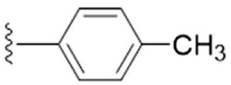	3.3833	±0.0927	1.8428	±0.0980
5c	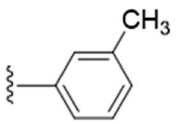	**1.3759**	**±0.1019**	**2.0164**	**±0.0538**
5d	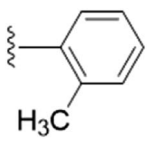	**0.9073**	**±0.0924**	**1.9723**	**±0.4236**
5e	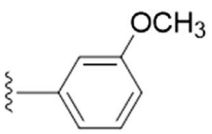	4.5737	±0.0995	1.8862	±0.2533
5f	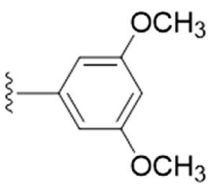	2.6508	±0.1694	2.3425	±0.0228
5g	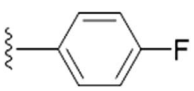	6.4687	±0.1334	1.4489	±0.1579
5h	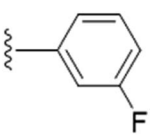	**1.5437**	**±0.0227**	**2.1015**	**±0.0315**
5i	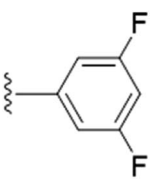	**1.5609**	**±0.0237**	**1.2138**	**±0.2832**
5j	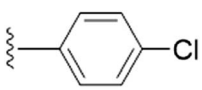	2.7187	±0.0435	1.9697	±0.1800

Table 1 (*Contd.*)

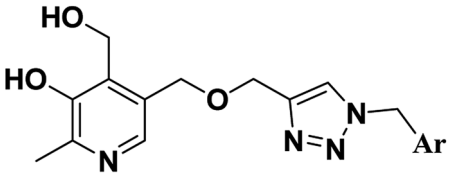

5

Compound	Ar	EeAChE IC_{50} ± SEM[a] (mM)		ORAC index ± SEM[b]	
5k	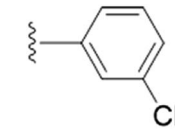	2.70723333	±0.0127	0.8358	±0.0374
5l	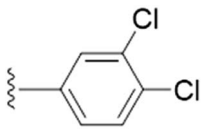	3.3777	±0.2162	1.9421	±0.1603
5m	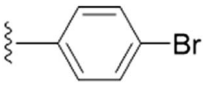	3.1383	±0.0432	1.215	±0.1383
5n	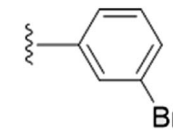	**1.0801**	**±0.0851**	**2.2079**	**±0.1003**
5o	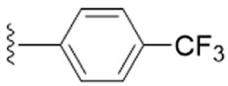	6.5162	±0.1326	2.0758	±0.1775
5p	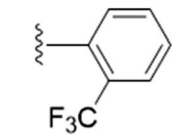	3.6525	±0.0120	0.8718	±0.2761
5q	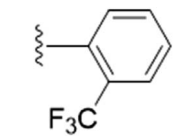	**1.1346**	**±0.1632**	**0.7168**	**±0.1410**
Pyridoxine	—	n.a[c]		0.5249	±0.1084
Donepezil	—	<5 μM		N.T[d]	
Trolox	—	N.T[d]		1	

[a] IC_{50} values is the concentration of the enzyme required to decrease the enzyme activity by 50% and are the mean of three independent experiments, represented in mean ± SEM (SEM = standard error mean). [b] The mean ± SEM of three independent experiments. Data are represented as ORAC-FL values of Trolox equivalents (μM of tested compound/μM of Trolox). [c] n.a = not active. [d] N.T = not tested.

another compound, chlorine at 3rd and 4th position (**5l**). Inclusion of two fluorine atoms at both the *meta* positions, did not show change in potency but there was a spurt in % of enzyme inhibition. To summarize the effect of di-substitution on the aromatic ring, **5i** was considered the best as compared to **5l** and **5f**. Owing to the fact that fluorine and methoxy groups are both ring activators, the difference in potency and percentage of inhibition between the two can be due to the high electronegativity and small size of fluorine.

We tried with trifluoro-methyl substitution at *para*, *meta* and *ortho* positions (**5o**, **5p**, **5q**). Trifluoro-methyl substitution at the *ortho* position was the best amongst the three both from the perspective of potency and inhibitory activity. However, when compared with methyl substitution, **5b** was double potent in

Table 2 Percentage of AChE inhibition of **5c**, **5d**, **5h**, **5i**, **5n**, **5q** and donepezil at different concentrations of the compounds[a]

	156 μM		312 μM		625 μM		1.25 mM		2.5 mM		5 mM		10 mM	
	%	±SEM	%	±SEM	%	±SEM	%	±SEM	%	±SEM	%	±SEM	%	±SEM
5c	22.49	3.62	26.92	0.55	39.11	2.48	53.8	3.13	64.11	1.79	73.43	1.13	81.92	0.85
5d	33.53	6.44	36.41	6.8	51.15	5.55	58.56	4	69.57	2.3	81.3	2.36	86.03	0.63
5h	19.04	0.29	25.49	2.22	35.1	1.59	56.37	1.85	60.48	1.24	66.56	0.26	69.02	0.36
5i	14.97	4.12	26.58	3.92	35.38	0.47	43	1.52	61.41	2.82	66.78	0.1	77.89	0.15
5n	14.69	1.15	25.79	2.73	41.99	1.42	57.39	4.99	70.16	4.11	75.88	2.44	86.28	1.38
5q	22.49	3.62	26.92	0.55	39.11	2.48	53.8	3.13	64.11	1.79	73.43	1.13	81.92	0.85
Donepezil	89.07	1.19	94.5	0.81	97.44	0.73	100.88	0.93	99.7	1.04	99.74	0.69	99.95	0.48

[a] Data presented here is of % of AChE inhibition mean ± SEM of three independent experiments at different concentrations. Donepezil is taken as the reference compound.

respect to **5o**. We got the same observation for *meta* substitution as well, **5c** was twice in terms of potency as compared to **5p**. Methyl substitution at the *ortho* position was marginally better in terms of trifluoro-methyl substitution at the same position. Methyl group is considered as ring activator, while trifluoro-methyl group as ring deactivator. Therefore, the observations confirm that EDG is best suited for inhibitory activity against AChE, when pyridoxine based triazoles are concerned. Table 2 gives a detailed information of percentage of inhibition of AChE at different concentrations of by **5c**, **5d**, **5h**, **5i**, **5n**, **5q** and the reference compound, donepezil. Fig. 3 shows the comparative results of percentage of inhibition of AChE by **5c**, **5d**, **5h**, **5i**, **5n**, **5q** derivatives at 10 mM concentration, taking donepezil as the reference standard.

To summarize all our observations with respect to our standard compound donepezil, our molecules required a higher concentration to show their inhibitory activity. Donepezil showed almost 89% inhibition at the highest dilution in which we tested our compounds (156 μM) and 65% inhibition at 5 μM. However, at the highest concentration, that is, at 10 mM concentration, compounds showed a maximum of 86% inhibitory activity towards AChE while donepezil exhibited 100% activity.

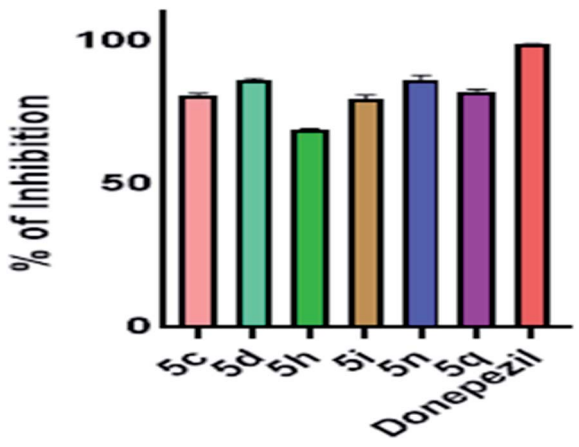

Fig. 3 Percentage of inhibition of AChE by **5c**, **5d**, **5h**, **5i**, **5n**, **5q** derivatives at 10 mM concentration. Data presented here is mean ± SEM of three independent experiments.

2.4 Antioxidant study

Aging is associated with oxidative stress resulting in generation of reactive oxygen species. We determined the oxygen radical absorption capacity-fluoroscein (ORAC-FL) values for the entire series. The ORAC-FL values are given in Table 1 and are a measure of the total antioxidant capacity. We generated peroxyl free radicals using the free radical generator 2,2-azobis(2-amidino-propane)dihydrochloride (AAPH) and fluorescein as the fluorescent probe in this assay at 37 °C. The total antioxidant capacity of the molecules were determined in equivalents to Trolox (vitamin E analogue), keeping both at same concentration (8 μM). One of the reasons for choosing pyridoxine as a pharmacophore was for it's antioxidant nature. We observed all our compounds to have anti-oxidant property as shown in Table 1.

Vitamin B_6 being a dietary supplement was tested using the ORAC-FL method. All the compounds showed almost similar anti-oxidant nature, however, pyridoxine showed the most efficacy in terms of an anti-oxidant. Pyridoxine was taken as a reference compound to evaluate the entire series in this experiment.

Therefore, from the observations of Table 1, we selected **5c**, **5d**, **5h**, **5i**, **5n** and **5q** on the basis of AChE inhibitory activity and antioxidant property of the compounds for further evaluations.

2.5 Metal chelation study

Chelation of bio-metals will make the compounds prove as MTDLs and be an added advantage. We tested **5c**, **5d**, **5h**, **5i**, **5n** and **5q** against bio-metals Fe^{3+}, Cu^{2+}, Zn^{2+}, Al^{3+} which are responsible for AD, using UV spectrophotometer within the wavelength range of 200 to 600 nm. All these bio-metals are responsible for the pathophysiological conditions in AD. We found a marked ability within the compounds to chelate Fe^{3+}. Compounds **5c**, **5i** and **5q** chelated both Fe^{3+} and Al^{3+}, **5i** chelated the metals most with a 222% increase in absorbance at 292 nm which also includes a bathochromic shift of about 3 nm in case of Fe^{3+} and an increase of 104% in absorbance at 292 nm which too included a bathochromic shift of 4 nm in case of Al^{3+}. The observations for all the compounds studied for metal chelation a study has been tabulated in Table 3.

Although, aluminium being the most abundant metal on the earth's crust, it do not pose an immediate health concern when being exposed to the human body. Chronic exposure to

aluminium in drinking water has been studied for it's association with AD. To add more to the pathophysiology, aluminium is known to enhance ROS generation and stimulated iron based generation of ROS species. Both these metals are also known to be associated with the senile plaques.[19] Therefore, **5i** has the ability to chelate both the trivalent cations which can add well to the property of the compound as a MTDL as shown in Fig. 4a.

The main challenge for chelation therapy of metals is selectivity towards metal cations. So we sought to check the selectivity towards essential metals responsible for proper physiological functions of our body. We included Ca^{2+}, Mg^{2+}, Na^{+} and K^{+} in our study and interestingly found out that **5i** did not chelate these metal ions at all (Fig. 4a). The spectrum of **5i**–Fe^{3+} complex was quite different from the parent spectrum and those by other metals. Owing to the fact, that our biological system comprise a mixture of metal ions, we sought to check the affinity of our compound **5i** towards Fe^{3+} in the presence of other metals (Fe^{3+}, Zn^{2+}, Cu^{2+}, Ca^{2+}, Mg^{2+}, Na^{+} and K^{+}) present in equal amount. However, we excluded Al^{3+} from the study as the purpose was to check affinity towards Fe^{3+} and Al^{3+} does not form an essential part of our system. We observed the characteristic curve of **5i**–Fe^{3+} as **5i** showed affinity towards Fe^{3+} in the metal pool (Fig. 4b).

We studied the stoichiometric association of the Fe^{3+}–**5i** complex by keeping the amount of ligand fixed and titrating the amount of metal in increasing concentration ranging from 0–100 μM using UV spectrophotometer. The spectral changes were recorded at nm and a graph was plotted (Fig. 4c). There was an increase in intensity at 293 nm and a decrease at 327 nm, on successive increase in concentration of Fe^{3+}. We analysed the data and plotted the Job's plot, at 239 nm and 327 nm where on extrapolation we got a mole fraction of 0.5 in both the wavelength confirming formation of 1 : 1 stoichiometric complex between **5i** and Fe^{3+} (Fig. 4d and e).

Good *et al.* performed a laser microprobe study or the LAMMA study where it was found selective deposition of Al and Fe in the neurofibrillary tangles.[20] Therefore, **5i** being a selective aluminium and iron chelator can be a potential inhibitor against these potentially toxic metals and can surely halt the mechanism of pathological important structures.

Table 3 Observations from metal chelation studies

		Cu^{2+}		Zn^{2+}		Al^{3+}		Fe^{3+}	
	Compound	% ΔA^a	Shift[b]	% ΔA^a	Shift[b]	% ΔA^a	Shift[b]	% ΔA^a	Shift[b]
5c									
λ_{max}	256.39	0	0	0	0	—	—	—	—
	287.7	0	0	0	0	(+)58.41	(−)4.76	(−)171.14	(−)6.22
	326.31	0	0	0	0	(+)141.5	(+)0.42	—	—
5d									
λ_{max}	254.28	(+)8.76	(−)1.21	(+)6.04	(−)1.21	(+)9.36	(−)1.21	(+)48.04	0
	288	(−)34.63	0	(−)34.62	(−)1	(−)31.94	(−)2	(−)1.19	(−)4
	324.35	(+)3.75	(+)0.79	(−)8.41	0	(−)7.13	(−)0.41	(−)21.00	0
5h									
λ_{max}	257.15	(−)10.20	(+)1.03	(+)17.14	(+)0.31	(+)11.02	0	(−)65.31	(+)0.67
	288.5	(−)9.15	(−)0.5	(+)20.42	(−)0.36	(+)3.52	(+)1.4	(−)105.63	(+)0.67
	325.74	(+)5.65	(+)0.74	(+)11.01	(−)0.26	(+)10.42	(−)0.26	(−)27.08	(+)0.36
5i									
λ_{max}	257.85	0	0	0	0	—	—	—	—
	288.78	0	0	0	0	(−)104.57	(−)3.68	(−)221.83	(−)2.6
	325.93	0	0	0	0	(+)43.01	(−)1.09	(+)48.38	(−)3.25
5n									
λ_{max}	254.72	(+)17.34	(−)1.09	(+)1.24	(−)1.08	(+)5.88	(−)1.08	(−)54.80	(−)0.72
	290.57	(+)18.93	(+)0.67	(+)2.43	(+)2.07	(+)5.82	(+)2.07	(−)70.39	(+)2.07
	324.71	(+)16.59	0	(+)4.255	(−)0.67	(+)4.25	(−)0.67	(−)23.62	(+)0.36
5q									
λ_{max}	258.23	0	0	0	0	—	—	—	—
	288.46	0	0	0	0	(−)78.07	(−)3.62	(−)185.50	(−)2.92
	325.56	0	0	0	0	(+)39.70	0	(+)47.94	0

[a] Data represented here is percentage change in absorbance; (+) indicating a decrease in absorbance and (−) as increase; calculated by the formula [(abs of tested compound − abs of complex)/abs of tested compound] × 100. [b] Data represented here is shift in nm; (+) indicates a hypsochromic shift and (−) indicates a bathochromic shift as calculated from the formula [λ_{max} of tested compound − λ_{max} of complex].

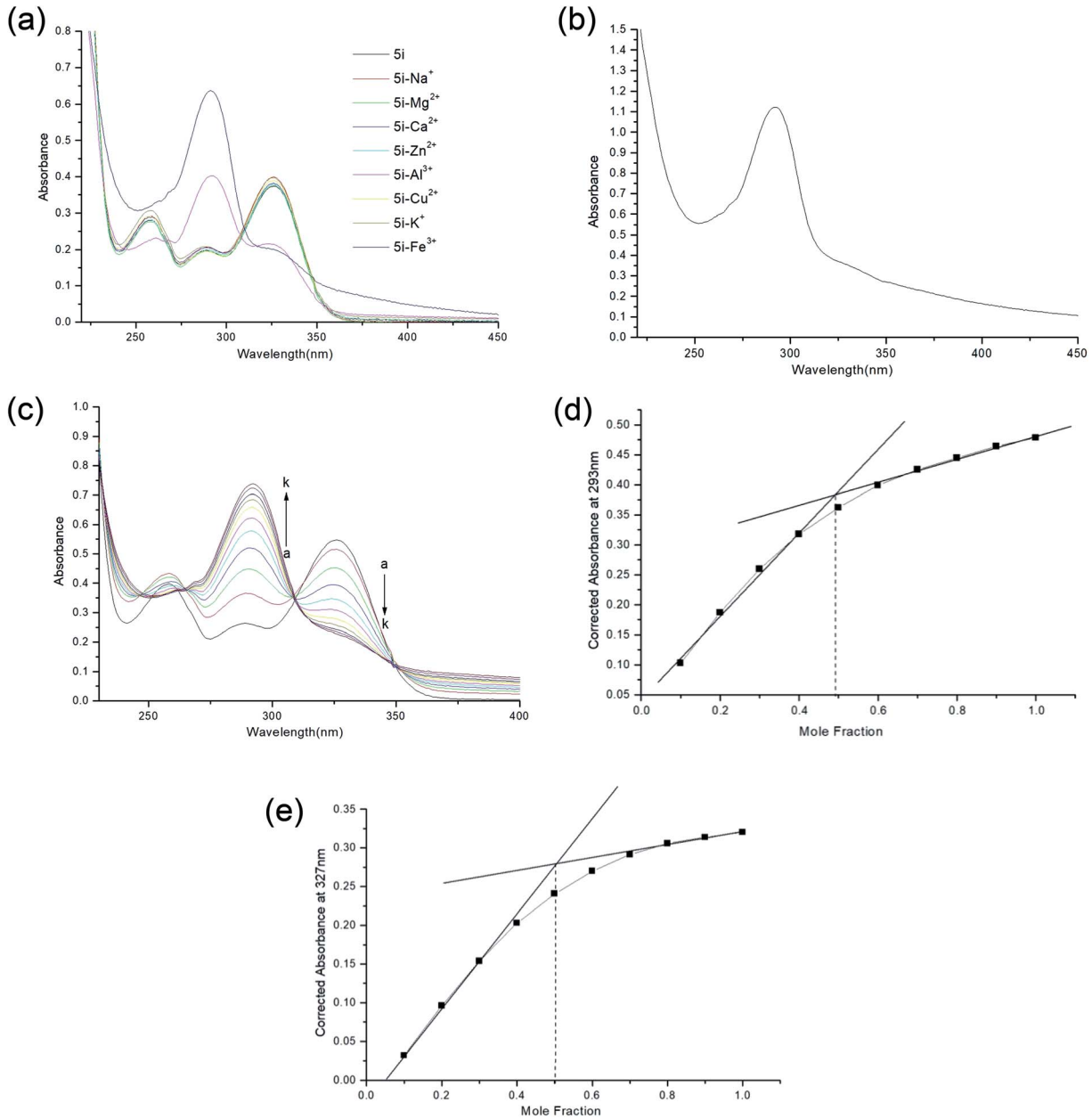

Fig. 4 (a) Metal chelation spectra of **5i**. (b) Selectivity spectrum of **5i** from metal pool comprising of Fe^{3+}, Zn^{2+}, Cu^{2+}, Ca^{2+}, Mg^{2+}, Na^{+} and K^{+}; **5i** formed complex with Fe^{3+} as identified from it's characteristic curve shown in (a). (c) Titration spectra of Fe^{3+} with **5i** with 20 μL aliquots of metal solution to in increase the concentration of Fe^{3+} from 0–100 μM [a–k], with successive increment of 10 μM. (d) Job's plot of **5i** at 293 nm. (e) Job's plot of **5i** at 327 nm.

2.6 *In silico* study

2.6.1 Molecular docking study. We investigated on the binding mode of pyridoxine based triazole derivatives with AChE. We studied the binding interaction of **5i** with AChE using molecular docking in Schrodinger glide. The Fig. 5 represents the molecular interactions of **5i** with the active site amino acid residues of the enzyme AChE. The molecular docking was done with recombinant human AChE (PDB ID 4EY5) and it's 2D representation has been shown in Fig. 5.[21] The interactions mainly observed were with the peripheral anionic site of the enzyme (PAS site) with hydrophobic amino acids Tyr 124 and Phe 338 having π–π interactions with triazole nucleus of **5i**. On the other hand, pyridine nucleus of the pyridoxine moiety was seen to have π–π interaction with hydrophobic Trp 286. The principal amino acid of PAS, that is, Trp 86, was found in the vicinity of the ligand.[22] The hydroxyl group of the pyridoxine was found to form hydrogen bond with Arg 296. The catalytic anionic site (CAS) amino acids Ser 203 and His 447 were found in close proximity of the ligand. The dock score of **5i** calculated from the molecular docking study was −8.50 kcal J^{-1}.

The ligand showed interactions with the PAS site amino acids of AChE and binding to the PAS site of the enzyme is known to inhibit Aβ aggregation due to the homologous domains of the β-neurexin with PAS site, itself serving as

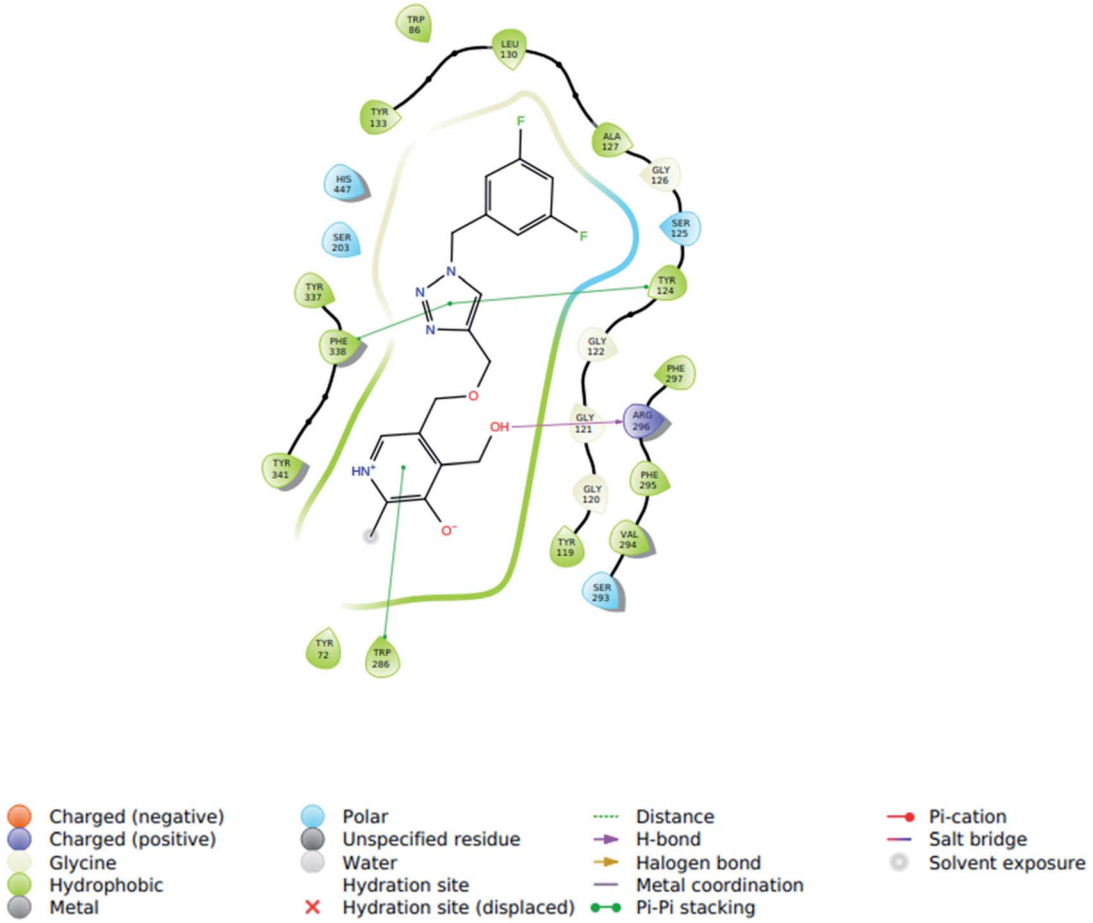

Fig. 5 2D representation of molecular docking study of **5i** with AChE (PDB ID 4EY5).

a ligand. Thus *in silico* results of molecular docking with ligand validated the results obtained from the *in vitro* AChE experiments.

2.6.2 Predictive ADME properties of 5i by computational methods. Taking the help of SwissADME (http://www.swissadme.ch), we predicted the drug-like properties, pharmacokinetic and physicochemical properties of **5i**. This open access web tool comprised proficient methods of predictive tools like BOILED EGG,[23] Bioavailability Radar. The software presents an early estimation of these ADME parameters (for Absorption, Distribution, Metabolism and Excretion) and provides sufficient light to the physicochemical parameters which is needed to be improved during formulation. The *in silico* result predicted by the aforesaid software is presented in Fig. 6a and b. The molecule **5i** was found to possess good drug likeness properties and was well within the Bioavailability Radar. The Bioavailability Radar gives a first glance of the drug-likeness of the molecule. The spider web like structure given inside Fig. 6a is the Bioavailability Radar. The pink region is the optimal range for every property. Daina *et al.* explained well about the web tool for prediction of drug likeness properties. All the predicted properties of the compound **5i** by the web tool have been put up in Fig. 6a.[24]

Fig. 6b is the BOILED EGG representation of the permeation properties of the molecule **5i**. The figure displays two parts, the white part representing those set of values which allows gastric permeation and the yolk or the yellow region representing those set of values which allows blood–brain-barrier permeation. The graph is plotted against *W* log *P*[*a* log *P*(*n*-octanol/water partition coefficient) method developed by Wildman and Crippen] *versus* TPSA or Topological Polar Surface Area in the BOILED EGG representation. The blue dot in the figure written as Molecule 1 is of **5i**.

2.6.3 Toxicity prediction of 5i by computational methods. The *in silico* toxicity prediction can reduce the time, cost and the number of animal experiments. We used the ProTox software for this *in silico* study, which identifies the LD_{50} value of the median lethal dose of a drug after analysing the similarity of the compounds and also identifies the toxic fragments.[25] It is an open access web tool (http://www.tox.charite.de/tox), which displays strong results at (sensitivity, specificity and precision of 76, 95 and 75%, respectively) which are validated by diverse external set. Fig. 7 displays the oral toxicity prediction results which show the molecule **5i** to have a predicted LD_{50} of 3350 mg kg^{-1}, falling under the Class 5 of toxicity of chemical classification. The molecule is predicted to be inactive in case of hepatotoxicity, carcinogenicity, mutagenicity, cytotoxicity, all

(a)

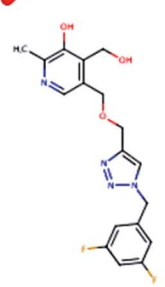

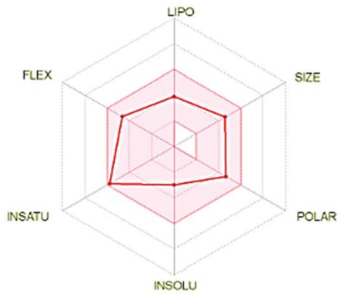

SMILES OCc1c(COCc2nnn(c2)Cc2cc(F)cc(c2)F)cnc(c1O)C

Physicochemical Properties	
Formula	C18H18F2N4O3
Molecular weight	376.36 g/mol
Num. heavy atoms	27
Num. arom. heavy atoms	17
Fraction Csp3	0.28
Num. rotatable bonds	7
Num. H-bond acceptors	8
Num. H-bond donors	2
Molar Refractivity	91.94
TPSA	93.29 Å²

Lipophilicity	
Log $P_{o/w}$ (iLOGP)	2.57
Log $P_{o/w}$ (XLOGP3)	1.31
Log $P_{o/w}$ (WLOGP)	2.61
Log $P_{o/w}$ (MLOGP)	1.30
Log $P_{o/w}$ (SILICOS-IT)	3.30
Consensus Log $P_{o/w}$	2.22

Water Solubility	
Log *S* (ESOL)	-3.00
Solubility	3.74e-01 mg/ml ; 9.94e-04 mol/l
Class	Soluble
Log *S* (Ali)	-2.87
Solubility	5.08e-01 mg/ml ; 1.35e-03 mol/l
Class	Soluble
Log *S* (SILICOS-IT)	-5.80
Solubility	6.02e-04 mg/ml ; 1.60e-06 mol/l
Class	Moderately soluble

Pharmacokinetics	
GI absorption	High
BBB permeant	No
P-gp substrate	Yes
CYP1A2 inhibitor	Yes
CYP2C19 inhibitor	No
CYP2C9 inhibitor	No
CYP2D6 inhibitor	Yes
CYP3A4 inhibitor	Yes
Log K_p (skin permeation)	-7.67 cm/s

Druglikeness	
Lipinski	Yes; 0 violation
Ghose	Yes
Veber	Yes
Egan	Yes
Muegge	Yes
Bioavailability Score	0.55

Medicinal Chemistry	
PAINS	0 alert
Brenk	0 alert
Leadlikeness	No; 1 violation: MW>350
Synthetic accessibility	3.07

(b)

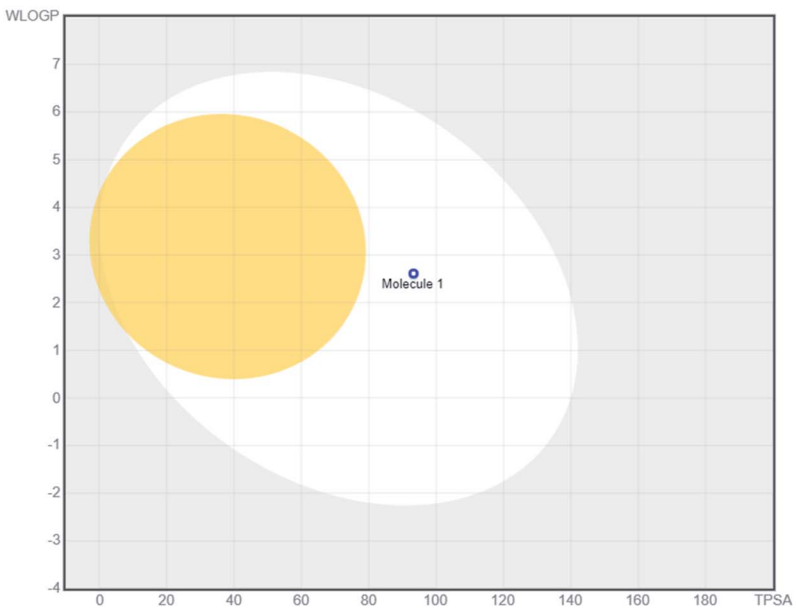

Fig. 6 (a) Predicted ADME properties of **5i** as obtained from the report generated by SwissADME software. (b) BOILED EGG representation of **5i** (denoted as Molecule 1 and represented by blue dot in the figure). From the BOILED EGG representation, the yolk denotes the points which allows passive blood–brain-barrier permeation, while the white region denotes points for passive gastrointestinal tract absorption. The graph is plotted against *W* log *P*[*a* log *P*(*n*-octanol/water partition coefficient) method developed by Wildman and Crippen] *versus* TPSA or Topological Polar Surface Area.

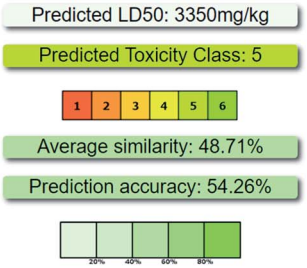

Toxicity Model Report

Classification	Target	Shorthand	Prediction	Probability
Organ toxicity	Hepatotoxicity	dili	Inactive	0.53
Toxicity end points	Carcinogenicity	carcino	Inactive	0.53
Toxicity end points	Immunotoxicity	immuno	Active	0.98
Toxicity end points	Mutagenicity	mutagen	Inactive	0.51
Toxicity end points	Cytotoxicity	cyto	Inactive	0.68
Tox21-Nuclear receptor signalling pathways	Aryl hydrocarbon Receptor (AhR)	nr_ahr	Inactive	0.76
Tox21-Nuclear receptor signalling pathways	Androgen Receptor (AR)	nr_ar	Inactive	0.94
Tox21-Nuclear receptor signalling pathways	Androgen Receptor Ligand Binding Domain (AR-LBD)	nr_ar_lbd	Inactive	0.98
Tox21-Nuclear receptor signalling pathways	Aromatase	nr_aromatase	Inactive	0.81
Tox21-Nuclear receptor signalling pathways	Estrogen Receptor Alpha (ER)	nr_er	Inactive	0.90
Tox21-Nuclear receptor signalling pathways	Estrogen Receptor Ligand Binding Domain (ER-LBD)	nr_er_lbd	Inactive	0.98
Tox21-Nuclear receptor signalling pathways	Peroxisome Proliferator Activated Receptor Gamma (PPAR-Gamma)	nr_ppar_gamma	Inactive	0.93
Tox21-Stress response pathways	Nuclear factor (erythroid-derived 2)-like 2/antioxidant responsive element (nrf2/ARE)	sr_are	Inactive	0.95
Tox21-Stress response pathways	Heat shock factor response element (HSE)	sr_hse	Inactive	0.95
Tox21-Stress response pathways	Mitochondrial Membrane Potential (MMP)	sr_mmp	Inactive	0.75
Tox21-Stress response pathways	Phosphoprotein (Tumor Supressor) p53	sr_p53	Inactive	0.91
Tox21-Stress response pathways	ATPase family AAA domain-containing protein 5 (ATAD5)	sr_atad5	Inactive	0.98

Fig. 7 Report of toxicity prediction as generated by ProTox-II online tool.

nuclear signalling pathways and stress response pathways. The predicted LD_{50} value of **5i** is well in correlation with the fact that pyridoxine itself rarely causes toxicity when given in very high doses. The *in silico* results generated gives us intuitive idea that **5i** can be considered as a much safer molecule.

3 Conclusion

Here, we report the design, synthesis and biological evaluations of a novel class of pyridoxine based triazole as multi-target directed ligands. Pyridoxine itself is very crucial for the homocysteine balance in AD patients and as well as considered an important vitamin for our daily diet. However, as proved from our experiment, it is not an AChE inhibitor. Out of the seventeen synthesized pyridoxine based triazoles, six showed good AChE inhibition and antioxidant potency. *Meta* and *ortho* substitution on the aromatic ring with EDG or ring activator proved beneficiary for AChE activity. With further metal chelation studies, we found **5i** as the best compound of this new series. **5i** has good AChE inhibitory activity ($IC_{50} = 1.56 \pm 0.02$ mM) with 77.89% of inhibition at highest concentration and possessed antioxidant property having ORAC-FL value of 1.21 ± 0.28 equivalent to Trolox, whose ORAC-FL value is taken as 1. The *in vitro* results for **5i** has been validated with the help of molecular docking with AChE by investigating it's binding poses. The compound **5i** chelated Fe^{3+} as the spectra showed about 220% increase in absorbance and a 104% increase was seen in case of Al^{3+}, exhibiting bathochromic shift in both. Selectivity towards targeted metal ion has always been a challenge in metal chelation therapeutics, henceforth, further throwing light on the ability of **5i** to selectively chelate Fe^{3+} from a pool of metal ions, gives it an added advantage. None of the literature of triazole based anti-Alzheimer's agents have reported selectivity towards metal ions with a drastic change in absorbance. We concluded our work with *in silico* studies of drug likeness, pharmacokinetic properties of **5i**, along with toxicity predictions which predicted it to be under Class 5 according to the toxicity labelling of chemicals. Our initial findings can open up new therapeutic areas in multi-target directed ligands against AD.

4 Experimental section

4.1 Chemistry

4.1.1 General remarks. All chemical reagents and solvents were purchased from Sigma Aldrich, Spectrochem Pvt. Ltd, Alfa Aesar and used without further purification. Reactions were monitored by Thin Layer Chromatography (TLC) using Merck silica gel 60 F254 pre-coated plates (0.25 mm) and the compounds were examined under UV chamber (Ultra violet fluorescence analysis cabinet-PSI). Column chromatography was performed with silica gel (100–200 mesh). All products were characterized by ^{1}H NMR, ^{13}C NMR and IR spectroscopy. ^{1}H, ^{19}F and ^{13}C NMR were recorded on JEOL RESONANCE ECZ500R at 500 MHz, 470 MHz and 125 MHz respectively with chemical shift (δ) expressed in parts per million in $CDCl_3$ at 27 °C downfield from TMS as an internal standard and coupling in Hertz (Hz). Splitting patterns are described as singlet (s),

doublet (d), triplet (t), multiplet (m), doublet of doublet (dd) and doublet of triplet (dt). For ^{1}H NMR, ^{13}C NMR reference for $CDCl_3$ appeared at 7.26 and 77.367 ppm respectively. For ^{1}H NMR, ^{13}C NMR reference for DMSO-d_6 appeared at 2.50 ppm and 39.52 ppm respectively. IR spectra were recorded on a BRUKER ECO-ATR Spectrometer. HRMS was measured on LC-MS by Agilent Technologies LC-MS and purity check was done using HPLC on a HPLC by Agilent Technologies. The retention time in HPLC is represented as t_R and calculated in minutes (min).

4.1.2 General procedure for the acetonide protection of (5-hydroxy-6-methylpyridine-3,4-diyl)dimethanol. To a suspension of pyridoxine hydrochloride (5.00 g, 24.3 mmol) in dry acetone (75 mL) under argon atmosphere, added 2,2-dimethoxypropane (50.1 mL, 408 mmol) and stirred for 10 min.[26] Following this, *p*-toluenesulfonic acid monohydrate (18.5 g, 97.2 mmol) was added and the reaction was stirred in room temperature for 20 hours. Completion of the reaction was monitored by TLC. The reaction mixture was neutralized with aqueous sodium bicarbonate, concentrated under reduced pressure, and the dark brown solution was extracted with dichloromethane (40 mL × 3). The organic phase was washed with brine and dried over anhydrous Na_2SO_4. The DCM layer was concentrated in vacuum to provide a crude product, which was washed with hexane to give compound **2** as white crystals in 86% yield.

4.1.2.1 (2,2,8-Trimethyl-4H-[1,3]dioxino[4,5-c]pyridin-5-yl) methanol (2). White solid crystals; mp-110–113 °C; $R_f = 0.5$ (ethyl acetate/hexane 3 : 2); ^{1}H NMR (500 MHz, chloroform-*d*) δ 7.77 (s, 1H, N=C<u>H</u>) δ 4.91 (s, 2H, O–C<u>H</u>$_2$) δ 4.52 (s, 2H, C<u>H</u>$_2$–OH) δ 2.34 (s, 3H, C<u>H</u>$_3$) δ 1.53 (s, 6H, 2 × C<u>H</u>$_3$); ^{13}C NMR (125 MHz, chloroform-*d*) δ 145.44, 145.09, 138.42, 130.59, 125.24, 99.41, 58.24, 57.88, 24.53, 18.24; IR (cm^{-1}) ν: 3851.17, 3619.70, 1695.98, 1213.27.

4.1.3 General procedure for synthesis of 2,2,8-trimethyl-5-((prop-2-yn-1-yloxy)methyl)-4*H*-[1,3]dioxino[4,5-*c*]pyridine. To a suspension of sodium hydride (1.5 eq.) in THF (40 mL), added (2,2,8-trimethyl-4*H*-[1,3]dioxino[4,5-*c*]pyridin-5-yl)methanol (**2**) (1.00 g, 4.7 mmol) under argon atmosphere and refluxed for 30 min. Following this, propargyl bromide (2 eq.) was added dropwise for 1 h and the reaction mixture was refluxed for 4 h. Completion of the reaction was monitored by TLC. The reaction mixture was concentrated under reduced pressure, quenched with saturated ammonium chloride solution and extracted with dichloromethane (40 mL × 3). The organic phase was washed with brine and dried over anhydrous Na_2SO_4. The DCM layer was concentrated in vacuum to provide a crude product, which was purified by column on silica using 20 : 80 ratio of hexane–DCM solvent system to provide compound **3** in 75% yield.

4.1.3.1 2,2,8-Trimethyl-5-((prop-2-yn-1-yloxy)methyl)-4H-[1,3] dioxino[4,5-c]pyridine (3). Brown oil; R_f = 0.6 (DCM/methanol 12 : 1); ^{1}H NMR (500 MHz, chloroform-*d*) δ 7.99 (s, 1H, N=C<u>H</u>) δ 4.9 (s, 2H, O–C<u>H</u>$_2$) δ 4.71 (s, 2H, C<u>H</u>$_2$–OH) δ 4.46 (s, 2H, C<u>H</u>$_2$–C) δ 2.4 (s, 3H, C<u>H</u>$_3$) δ 1.5 (s, 6H, 2 × C<u>H</u>$_3$); IR (cm^{-1}) ν: 3292.03, 2992.75, 2931.93, 2858.50, 2114.38, 1067.29, 1025.50.

4.1.4 General procedure for synthesis of substituted 5-(((1-benzyl-1*H*-1,2,3-triazol-4-yl)methoxy)methyl)-2,2,8-trimethyl-4*H*-[1,3]dioxino[4,5-*c*]pyridine 4(a–q). Different derivatives were prepared *via* the reaction of benzyl bromides (1.1 mmol) with sodium azide (1 mmol) in the presence of triethylamine in *t*-BuOH/water (1 : 1). After around 30 min, 2,2,8-trimethyl-5-((prop-2-yn-1-yloxy)methyl)-4*H*-[1,3]dioxino[4,5-*c*]pyridine (**3**) (1 mmol) in absolute *t*-BuOH (1 mL) was added to the solution in the presence of $CuSO_4 \cdot 5H_2O$ (10 mol%) and freshly prepared ascorbic acid solution (25 mol%), at 50 °C and stirred at 70 °C for 12 h. After completion of the reaction (checked by using TLC), the reaction mixture was passed through a slurry of Celite in ethyl acetate. The filtrate was concentrated under reduced pressure. The organic residue was extracted with EtOAc (20 mL × 3). The organic phase was washed with brine and dried over anhydrous Na_2SO_4. The solvent was evaporated to dryness under reduced pressure to afford compounds **4(a–q)**. The compounds were finally washed with hexane.

4.1.5 General procedure for deprotection of compounds 4(a–q). The corresponding compounds **4(a–q)** (0.60–0.65 mmol) was dissolved in THF (5 mL), and 10% HCl solution (4 mL) was added. The reaction mixture was refluxed for 6–11 h under an argon atmosphere. After complete reaction, THF was evaporated under reduced pressure. The residue was neutralized with aqueous saturated sodium bicarbonate solution, and extracted with EtOAc (20 mL × 3). The organic phase was washed with brine and dried over anhydrous Na_2SO_4. The solvent was evaporated to dryness under reduced pressure to **5(a–q)** in 85–96% yield. The compounds were finally washed with hexane.

4.1.5.1 5-(((1-Benzyl-1H-1,2,3-triazol-4-yl)methoxy)methyl)-4-(hydroxymethyl)-2-methylpyridin-3-ol (5a). Brown oil; yield 95%; R_f = 0.4 (DCM/methanol 19 : 1); ^{1}H NMR (500 MHz, chloroform-*d*) δ 7.75 (s, 1H, N=C<u>H</u>) δ 7.39 (s, 1H, C=C<u>H</u>–N) δ 7.36–7.31 (m, 3H, Ar–<u>H</u>) δ 7.21 (dd, J = 7.2, 2.2, 2H, Ar–<u>H</u>) δ 5.45 (s, 2H, N–C<u>H</u>$_2$) δ 4.95 (s, 2H, C<u>H</u>$_2$–O) δ 4.43 (s, 2H, C<u>H</u>$_2$–OH) δ 4.43 (s, 2H, C<u>H</u>$_2$–O) δ 2.40 (s, 3H, N–C–C<u>H</u>$_3$); ^{13}C NMR (125 MHz, chloroform-*d*) δ 152.05, 148.52, 144.80, 139.90, 134.26, 131.57, 129.28, 128.21, 127.54, 122.73, 68.25, 62.28, 59.77, 54.38, 18.67; IR (cm^{-1}) ν: 3141.08, 2926.77, 2863.95, 2363.77, 2246.90, 1615.93, 1225.02, 1213.27; HRMS (*m*/*z*): calculated for $C_{18}H_{20}N_4O_3$ [M + H]$^+$ 341.1691; found, 341.1611; HPLC purity-99%; t_R = 9.86 min.

4.1.5.2 4-(Hydroxymethyl)-2-methyl-5-(((1-(4-methylbenzyl)-1H-1,2,3-triazol-4-yl)methoxy)methyl)pyridin-3-ol (5b). Yellow sticky solid; yield 88%; R_f = 0.4 (DCM/methanol 19 : 1); ^{1}H NMR (500 MHz, chloroform-*d*) δ 7.83 (s, 1H, N=C<u>H</u>) δ 7.35 (s, 1H, C=C<u>H</u>–N) δ = 7.14 (q, J = 8.1, 4H, Ar–<u>H</u>) δ 5.42 (s, 2H, N–C<u>H</u>$_2$) δ 4.97 (s, 2H, C<u>H</u>$_2$–OH) δ 4.52 (s, 2H, C<u>H</u>$_2$–O) δ 4.42 (s, 2H, C<u>H</u>$_2$–O) δ 2.45 (s, 3HN–C–C<u>H</u>$_3$), δ 2.33 (s, 3H, Ar–C<u>H</u>$_3$); ^{13}C NMR (125 MHz, chloroform-*d*) δ 144.76, 140.56, 139.15, 134.72, 131.53, 131.29, 130.05, 129.94, 128.28, 122.42, 68.35, 61.47, 59.67, 54.22, 21.23, 18.85. IR (cm^{-1}) ν: 3145.19, 2930.77, 2869.75, 2367.37, 2248.92, 1620.39, 1221.03, 1210.28; HRMS (*m*/*z*): calculated for $C_{19}H_{23}N_4O_3$ [M + H]$^+$ 355.1770; found, 355.1772; HPLC purity-97%; t_R = 11.20 min.

4.1.5.3 4-(Hydroxymethyl)-2-methyl-5-(((1-(3-methylbenzyl)-1H-1,2,3-triazol-4-yl)methoxy)methyl)pyridin-3-ol (5c). Yellow oil; yield 87%; R_f = 0.4 (DCM/methanol 19 : 1); ^{1}H NMR (500 MHz, chloroform-*d*) δ 7.83 (s, 1H, N=C<u>H</u>) δ 7.37 (s, 1H, C=C<u>H</u>–N) δ 7.24–7.21 (m, 1H, Ar–<u>H</u>) δ = 7.16 (d, J = 7.6 Hz, 1H, Ar–<u>H</u>) δ 7.05–7.02 (m, 2H, Ar–<u>H</u>) δ 5.42 (s, 2H, N–C<u>H</u>$_2$) δ 4.97 (s, 2H,

CH_2–OH) δ 4.52 (s, 2H, CH_2–O) δ 4.43 (s, 2H, CH_2–O) δ 2.45 (s, 3H, N–C–CH_3), δ 2.32 (s, 3H, Ar–CH_3); ^{13}C NMR (125 MHz, chloroform-*d*) δ 140.38, 139.18, 134.11, 131.64, 129.78, 129.16, 128.97, 127.45, 125.67, 125.31, 122.58, 68.34, 61.68, 59.60, 54.43, 21.39, 18.75. IR (cm^{-1}) ν: 3146.20, 2931.47, 2868.75, 2369.58, 2249.22, 1622.19, 1223.10, 1211.32; HRMS (*m*/*z*): calculated for $C_{19}H_{23}N_4O_3$ $[M + H]^+$ 355.1770; found, 355.1768; HPLC purity-96%; t_R = 10.30 min.

*4.1.5.4 4-(Hydroxymethyl)-2-methyl-5-(((1-(2-methylbenzyl)-1H-1,2,3-triazol-4-yl)methoxy)methyl)pyridin-3-ol (**5d**).* Dark-green semisolid; yield 93%; R_f = 0.4 (DCM/methanol 19 : 1); ^{1}H NMR (500 MHz, chloroform-*d*) δ 7.83 (s, 1H, N=C**H**) δ 7.29 (s, 1H, C=C**H**–N) δ = 7.30–7.25 (m, 1H, Ar–**H**), δ 7.20 (dd, J = 7.2, 3.6 Hz, 2H, Ar–**H**), δ 7.13 (d, J = 8.0, 1H, Ar–**H**) δ 5.48 (s, 2H, N–CH_2) δ 4.97 (s, 2H, CH_2–OH) δ 4.52 (s, 2H, CH_2–O) δ 4.42 (s, 2H, CH_2–O) δ 2.45 (s, 3H, N–C–CH_3), δ 2.24 (s, 3H, Ar–CH_3); ^{13}C NMR (125 MHz, chloroform-*d*) δ 148.80, 143.86, 137.03, 132.11, 131.21, 129.61, 129.44, 126.83, 68.39, 61.62, 59.57, 52.56, 19.04; IR (cm^{-1}) ν: 3147.20, 2930.70, 2870.59, 2372.85, 2247.31, 1620.20, 1221.70, 1215.36; HRMS (*m*/*z*): calculated for $C_{19}H_{23}N_4O_3$ $[M + H]^+$ 355.1770; found, 355.1774; HPLC purity-95%; t_R = 10.92 min.

*4.1.5.5 4-(Hydroxymethyl)-5-(((1-(3-methoxybenzyl)-1H-1,2,3-triazol-4-yl)methoxy)methyl)-2-methylpyridin-3-ol (**5e**).* Yellow sticky solid; yield 90%; R_f = 0.4 (DCM/methanol 19 : 1); ^{1}H NMR (500 MHz, chloroform-*d*) δ 7.78 (s, 1H, N=C**H**) δ 7.40 (s, 1H, C=C**H**–N) δ 7.27 (d, J = 7.6 Hz, 1H, Ar–**H**) δ 6.86 (dd, J = 8.3, 2.5 Hz, 1H, Ar–**H**) δ 6.80 (d, J = 7.5 Hz, 1H, Ar–**H**) δ 6.74 (d, J = 1.6 Hz, 1H, Ar–**H**) δ 5.42 (s, 2H, N–CH_2) δ 4.96 (s, 2H, CH_2–OH) δ 4.46 (s, 2H, CH_2–O) δ 4.43 (s, 2H, CH_2–O) δ 3.75 (s, 3H, Ar–O–CH_3), δ 2.42 (s, 3H, N–C–CH_3); ^{13}C NMR (125 MHz, chloroform-*d* and DMSO-d_6) δ 156.30, 149.66, 144.88, 140.99, 134.97, 127.76, 124.99, 118.81, 118.55, 72.91, 68.02, 64.64, 60.09, 58.73, 23.86; IR (cm^{-1}) ν: 3248.36, 2932.56, 2873.62, 2375.56, 2248.32, 1620.20, 1231.80, 1218.36; HRMS (*m*/*z*): calculated for $C_{19}H_{23}N_4O_4$ $[M + H]^+$ 371.1719; found, 371.1719; HPLC purity-96%; t_R = 10.24 min.

*4.1.5.6 5-(((1-(3,5-Dimethoxybenzyl)-1H-1,2,3-triazol-4-yl)methoxy)methyl)-4-(hydroxymethyl)-2-methylpyridin-3-ol (**5f**).* Yellow oil; yield 85%; R_f = 0.4 (DCM/methanol 19 : 1); ^{1}H NMR (500 MHz, chloroform-*d*) δ 7.83 (s, 1H, N=C**H**) δ 7.41 (s, 1H, C=C**H**–N) δ 7.25 (s, 1H, Ar–**H**) δ 6.40 (s, 1H, Ar–**H**), δ 6.36 (s, 1H, Ar–**H**), δ 5.39 (s, 2H, N–CH_2) δ 4.96 (s, 2H, CH_2–OH) δ 4.50 (s, 2H, CH_2–O) δ 4.44 (s, 2H, CH_2–O) δ 3.74 (s, 6H, Ar–O–CH_3), δ 2.44 (s, 3H, N–C–CH_3); ^{13}C ^{13}C NMR (125 MHz, chloroform-*d* and DMSO-d_6) δ 161.43, 136.37, 127.44, 122.72, 106.32, 100.48, 68.30, 61.88, 59.74, 55.54, 54.41, 18.79.; IR (cm^{-1}) ν: 3245.63, 2893.60, 2892.36, 2376.78, 2369.32, 1623.20, 1241.81, 1278.23; HRMS (*m*/*z*): calculated for $C_{20}H_{25}N_4O_5$ $[M + H]^+$ 401.1825; found, 401.1834; HPLC purity-97%; t_R = 10.72 min.

*4.1.5.7 5-(((1-(4-Fluorobenzyl)-1H-1,2,3-triazol-4-yl)methoxy)methyl)-4-(hydroxymethyl)-2-methylpyridin-3-ol (**5g**).* Brown oil; yield 93%; R_f = 0.4 (DCM/methanol 19 : 1); ^{1}H NMR (500 MHz, chloroform-*d*) δ 7.82 (s, 1H, N=C**H**) δ 7.38 (s, 1H, C=C**H**–N) δ 7.24–7.20 (m, 2H, Ar–**H**), δ 7.03 (t, J = 8.6 Hz, 2H, Ar–**H**) δ 5.44 (s, 2H, N–CH_2) δ 4.98 (s, 2H, CH_2–OH) δ 4.51 (s, 2H, CH_2–O) δ 4.44 (s, 2H, CH_2–O) δ 2.44 (s, 3H, N–C–CH_3); ^{13}C NMR (125 MHz, chloroform-*d*) δ 148.67, 145.34, 140.30, 131.58, 130.16, 130.09, 122.49, 116.41, 116.24, 68.38, 61.78, 59.64, 53.64, 18.75; ^{19}F NMR (470 MHz, chloroform-*d*) δ −112.10 to −112.17 (m); IR (cm^{-1}) ν: 3247.63, 2896.70, 2912.86, 2378.87, 2367.85, 1613.10, 1245.81, 1218.23; HRMS (*m*/*z*): calculated for $C_{18}H_{20}N_4O_3F$ $[M + H]^+$ 359.1519; found, 359.1514; HPLC purity-99.8%; t_R = 10.32 min.

*4.1.5.8 5-(((1-(3-Fluorobenzyl)-1H-1,2,3-triazol-4-yl)methoxy)methyl)-4-(hydroxymethyl)-2-methylpyridin-3-ol (**5h**).* Yellow oil; yield 86%; R_f = 0.4 (DCM/methanol 19 : 1); ^{1}H NMR (500 MHz, chloroform-*d*) δ 7.81 (s, 1H, N=C**H**) δ 7.42 (s, 1H, C=C**H**–N) δ 7.33 (td, J = 8.0, 5.9 Hz, 1H, Ar–**H**), δ 7.06–6.99 (m, 2H, Ar–**H**) δ 6.92 (d, J = 9.1 Hz, 1H, Ar–**H**) δ 5.47 (s, 2H, N–CH_2) δ 4.98 (s, 2H, CH_2–OH) δ 4.51 (s, 2H, CH_2–O) δ 4.45 (s, 2H, CH_2–O) δ 2.44 (s, 3H, N–C–CH_3); ^{13}C NMR (125 MHz, chloroform-*d*) δ 151.98, 148.68, 145.06, 140.25, 131.55, 131.00, 130.94, 127.45, 123.65, 122.69, 116.15, 115.99, 115.24, 115.07, 68.37, 61.86, 59.69, 53.72, 18.73; ^{19}F NMR (470 MHz, chloroform-*d*) δ −111.20 (ddd, J = 9.0, 6.3, 2.2 Hz); IR (cm^{-1}) ν: 3245.63, 2893.70, 2911.86, 2375.77, 2377.65, 1619.20, 1286.81, 1220.23; HRMS (*m*/*z*): calculated for $C_{18}H_{20}N_4O_3F$ $[M + H]^+$ 359.1519; found, 359.1519; HPLC purity-98%; t_R = 10.30 min.

*4.1.5.9 5-(((1-(3,5-Difluorobenzyl)-1H-1,2,3-triazol-4-yl)methoxy)methyl)-4-(hydroxymethyl)-2-methylpyridin-3-ol (**5i**).* Yellow sticky solid; yield 96%; R_f = 0.3 (DCM/methanol 19 : 1); ^{1}H NMR (500 MHz, chloroform-*d* + DMSO-d_6) δ 7.87 (s, 1H, N=C**H**) δ 7.48 (s, 1H, C=C**H**–N) δ 6.85–6.79 (m, 3H, Ar–**H**), δ 5.56 (s, 2H, N–CH_2) δ 4.91 (s, 2H, CH_2–OH) δ 4.60 (s, 2H, CH_2–O) δ 4.52 (s, 2H, CH_2–O) δ 2.42 (s, 3H, N–C–CH_3); ^{13}C NMR (125 MHz, chloroform-*d* and DMSO-d_6) δ 156.20, 149.88, 144.87, 143.80, 135.68, 132.50, 128.31, 115.92, 115.71, 108.78, 72.95, 68.04, 64.48, 57.54, 23.92; ^{19}F NMR (470 MHz, chloroform-*d*) δ −103.42 to −103.51 (m); IR (cm^{-1}) ν: 3240.35, 2885.91, 2900.62, 2378.85, 2378.63, 1622.31, 1278.78, 1223.73; HRMS (*m*/*z*): calculated for $C_{18}H_{19}N_4O_3F_2$ $[M + H]^+$ 377.1425; found, 377.1422; HPLC purity-100%; t_R = 10.88 min.

*4.1.5.10 5-(((1-(4-Chlorobenzyl)-1H-1,2,3-triazol-4-yl)methoxy)methyl)-4-(hydroxymethyl)-2-methylpyridin-3-ol (**5j**).* Yellow sticky solid; yield 85%; R_f = 0.4 (DCM/methanol 19 : 1); ^{1}H NMR (500 MHz, chloroform-*d*) δ 7.80 (s, 1H, N=C**H**) δ 7.40 (s, 1H, C=C**H**–N) δ 7.32 (d, J = 8.4 Hz, 2H, Ar–**H**), δ 7.16 (d, J = 8.3 Hz, 2H, Ar–**H**) δ 5.43 (s, 2H, N–CH_2) δ 4.97 (s, 2H, CH_2–OH) δ 4.48 (s, 2H, CH_2–O) δ 4.44 (s, 2H, CH_2–O) δ 2.43 (s, 3H, N–C–CH_3); ^{13}C NMR (125 MHz, chloroform-*d*) δ 148.53, 145.03, 139.96, 135.10, 132.76, 131.63, 129.53, 129.50, 127.57, 122.62, 68.32, 62.04, 59.72, 53.62, 29.78, 18.65; IR (cm^{-1}) ν: 3224.69, 2895.81, 2910.25, 2376.68, 2379.36, 1627.91, 1278.70, 1210.35; HRMS (*m*/*z*): calculated for $C_{18}H_{20}N_4O_3Cl$ $[M + H]^+$ 375.1224; found, 375.1222; HPLC purity-97%; t_R = 11.56 min.

*4.1.5.11 5-(((1-(3-Chlorobenzyl)-1H-1,2,3-triazol-4-yl)methoxy)methyl)-4-(hydroxymethyl)-2-methylpyridin-3-ol (**5k**).* Yellow oil; yield 88%; R_f = 0.4 (DCM/methanol 19 : 1); ^{1}H NMR (500 MHz, chloroform-*d*) δ 7.84 (s, 1H, N=C**H**) δ 7.42 (s, 1H, C=C**H**–N) δ 7.34–7.27 (m, 2H, Ar–**H**), δ 7.23 (s, 1H, Ar–**H**) δ 7.10 (d, J = 7.2 Hz, 1H) δ 5.45 (s, 2H, N–CH_2) δ 4.99 (s, 2H, CH_2–OH) δ 4.54 (s, 2H, CH_2–O) δ 4.45 (s, 2H, CH_2–O) δ 2.45 (s, 3H, N–C–CH_3); ^{13}C NMR (125 MHz, chloroform-*d*) δ 151.92, 149.51, 148.78,

145.10, 130.60, 129.26, 128.25, 126.24, 122.65, 68.43, 61.68, 59.66, 53.67, 18.81; IR (cm^{-1}) ν: 3220.69, 2898.81, 2914.38, 2369.82, 2381.41, 1628.85, 1280.01, 1210.56; HRMS (*m*/*z*): calculated for $C_{18}H_{20}N_4O_3Cl$ $[M + H]^+$ 375.1229; found, 375.1225; HPLC purity-97%; $t_R = 10.32$ min.

*4.1.5.12 5-(((1-(3,4-Dichlorobenzyl)-1H-1,2,3-triazol-4-yl) methoxy)methyl)-4-(hydroxymethyl)-2-methylpyridin-3-ol (**5l**).* Yellow oil; yield 92%; $R_f = 0.4$ (DCM/methanol 19 : 1); ^{1}H NMR (500 MHz, chloroform-*d* + DMSO-d_6) δ 7.75 (s, 1H, N=C<u>H</u>) δ 7.64 (s, 1H, C=C<u>H</u>–N) δ 7.24–7.20 (m, 2H, Ar–<u>H</u>), δ 7.06 (s, 1H, Ar–<u>H</u>) δ 5.40 (s, 2H, N–C<u>H</u>$_2$) δ 4.78 (s, 2H, C<u>H</u>$_2$–OH) δ 4.48 (s, 2H, C<u>H</u>$_2$–O) δ 4.38 (s, 2H, C<u>H</u>$_2$–O) δ 2.30 (s, 3H, N–C–C<u>H</u>$_3$); ^{13}C NMR (125 MHz, chloroform-*d* and DMSO-d_6) δ 135.45, 131.07, 130.10, 127.62, 123.37, 68.19, 64.43, 59.76, 52.57, 19.27; IR (cm^{-1}) ν: 3225.72, 2890.23, 2926.83, 2370.82, 2380.62, 1629.85, 1282.01, 1217.61; HRMS (*m*/*z*): calculated for $C_{18}H_{19}N_4O_3Cl_2$ $[M + H]^+$ 410.0912; found, 410.0865; HPLC purity-98%; $t_R = 10.32$ min.

*4.1.5.13 5-(((1-(4-Bromobenzyl)-1H-1,2,3-triazol-4-yl)methoxy) methyl)-4-(hydroxymethyl)-2-methylpyridin-3-ol (**5m**).* Yellow sticky solid; yield 91%; $R_f = 0.6$ (DCM/methanol 19 : 1); ^{1}H NMR (500 MHz, chloroform-*d*) δ 7.84 (s, 1H, N=C<u>H</u>) δ 7.49 (d, J = 8.3 Hz, 2H, Ar–<u>H</u>) δ 7.48 (s, 1H, C=C<u>H</u>–N) δ 7.11 (d, $J = 8.3$, 2H, Ar–<u>H</u>) δ 5.43 (s, 2H, N–C<u>H</u>$_2$) δ 4.98 (s, 2H, C<u>H</u>$_2$–OH) δ 4.53 (s, 2H, C<u>H</u>$_2$–O) δ 4.44 (s, 2H, C<u>H</u>$_2$–O) δ 2.45 (s, 3H, N–C–C<u>H</u>$_3$) ^{13}C NMR (125 MHz, chloroform-*d*) δ 148.75, 133.25, 132.48, 129.80, 123.24, 122.56, 68.42, 61.70, 59.64, 53.69, 29.78; IR (cm^{-1}) ν: 3226.24, 2892.83, 2924.81, 2374.22, 2386.92, 1685.23, 1280.81, 1216.56; HRMS (*m*/*z*): calculated for $C_{18}H_{20}N_4O_3Br$ $[M + H]^+$ 419.0719; found, 419.0715; HPLC purity-99%; $t_R = 11.91$ min.

*4.1.5.14 5-(((1-(3-Bromobenzyl)-1H-1,2,3-triazol-4-yl)methoxy) methyl)-4-(hydroxymethyl)-2-methylpyridin-3-ol (**5n**).* Yellow oil; yield 91%; $R_f = 0.6$ (DCM/methanol 19 : 1); ^{1}H NMR (500 MHz, chloroform-*d*) δ 7.85 (s, 1H, N=C<u>H</u>) δ 7.48 (s, 1H, C=C<u>H</u>–N) δ 7.41 (d, $J = 8.3$ Hz, 2H, Ar–<u>H</u>) δ 7.23 (s, 1H, Ar–<u>H</u>) δ 7.15 (d, J = 7.7, 1H, Ar–<u>H</u>) δ 5.44 (s, 2H, N–C<u>H</u>$_2$) δ 4.98 (s, 2H, C<u>H</u>$_2$–OH) δ 4.53 (s, 2H, C<u>H</u>$_2$–O) δ 4.45 (s, 2H, C<u>H</u>$_2$–O) δ 2.45 (s, 3H, N–C–C<u>H</u>$_3$); ^{13}C NMR (125 MHz, chloroform-*d*) δ 132.20, 131.15, 130.85, 126.72, 123.30, 117.51, 68.44, 61.74, 59.67, 53.60, 36.88 IR (cm^{-1}) ν: 3225.20, 2890.63, 2923.72, 2373.15, 2388.85, 1685.57, 1282.74, 1210.78; HRMS (*m*/*z*): calculated for $C_{18}H_{20}N_4O_3Br$ $[M + H]^+$ 419.0719; found, 419.0715; HPLC purity-95%; $t_R = 11.79$ min.

*4.1.5.15 4-(Hydroxymethyl)-2-methyl-5-(((1-(4-(tri-fluoromethyl)benzyl)-1H-1,2,3-triazol-4-yl)methoxy)methyl) pyridin-3-ol (**5o**).* Yellow sticky solid; yield 95%; $R_f = 0.4$ (DCM/methanol 19 : 1); ^{1}H NMR (500 MHz, chloroform-*d*) δ 7.80 (s, 1H, N=C<u>H</u>) δ 7.62 (d, $J = 8.2$ Hz, 2H, Ar–<u>H</u>) δ 7.43 (s, 1H, C=C<u>H</u>–N) 7.33 (d, $J = 8.1$, 2H, Ar–<u>H</u>) δ 5.53 (s, 2H, N–C<u>H</u>$_2$) δ 4.98 (s, 2H, C<u>H</u>$_2$–OH) δ 4.49 (s, 2H, C<u>H</u>$_2$–O) δ 4.45 (s, 2H, C<u>H</u>$_2$–O) δ 2.43 (s, 3H, N–C–C<u>H</u>$_3$); ^{13}C NMR (125 MHz, chloroform-*d*) δ 151.97, 148.67, 145.22, 140.19, 138.21, 131.49, 128.35, 127.46, 126.26, 122.75, 68.40, 61.94, 59.72, 53.67, 18.74; ^{19}F NMR (470 MHz, chloroform-*d*) δ −62.71 (s); IR (cm^{-1}) ν: 3115.52, 2895.96, 2925.63, 2375.38, 2390.58, 1182.06, 1683.57, 1281.54, 1213.61; HRMS (*m*/*z*): calculated for $C_{19}H_{20}N_4O_3F_3$ $[M + H]^+$ 409.1488; found, 409.1489; HPLC purity-97%; $t_R = 12.57$ min.

*4.1.5.16 4-(Hydroxymethyl)-2-methyl-5-(((1-(3-(tri-fluoromethyl)benzyl)-1H-1,2,3-triazol-4-yl)methoxy)methyl) pyridin-3-ol (**5p**).* Yellow oil; yield 87%; $R_f = 0.4$ (DCM/methanol 19 : 1); ^{1}H NMR (500 MHz, chloroform-*d*) δ 7.82 (s, 1H, N=C<u>H</u>) δ 7.62 (s, 1H, C=C<u>H</u>–N) δ 7.51 (d, $J = 4.4$ Hz, 1H, Ar–<u>H</u>) δ 7.49 (d, $J = 7.8$ Hz, 1H, Ar–<u>H</u>) δ 7.44 (s, 1H, Ar–<u>H</u>) δ 7.41 (d, $J = 7.7$ Hz, 1H, Ar–<u>H</u>) δ 5.54 (s, 2H, N–C<u>H</u>$_2$) δ 4.98 (s, 2H, C<u>H</u>$_2$–OH) δ 4.52 (s, 2H, C<u>H</u>$_2$–O) δ 4.46 (s, 2H, C<u>H</u>$_2$–O) δ 2.44 (s, 3H, N–C–C<u>H</u>$_3$) ^{13}C NMR (125 MHz, chloroform-*d*) δ 140.23, 140.11, 135.32, 131.44, 129.95, 125.88, 124.84, 122.68, 68.40, 59.69, 53.74, 29.78; ^{19}F NMR (470 MHz, chloroform-*d*) δ −62.64 (s); IR (cm^{-1}) ν: 3116.27, 2896.56, 2923.18, 2374.38, 2391.60, 1180.28, 1682.66, 1280.45, 1216.68; HRMS (*m*/*z*): calculated for $C_{19}H_{20}N_4O_3F_3$ $[M + H]^+$ 409.1488; found, 409.1492; HPLC purity-96%; $t_R = 8.70$ min.

*4.1.5.17 4-(Hydroxymethyl)-2-methyl-5-(((1-(2-(tri-fluoromethyl)benzyl)-1H-1,2,3-triazol-4-yl)methoxy)methyl) pyridin-3-ol (**5q**).* Brown oil; yield 89%; $R_f = 0.4$ (DCM/methanol 19 : 1); ^{1}H NMR (500 MHz, chloroform-*d*) δ 7.82 (s, 1H, N=C<u>H</u>) δ 7.62 (s, 1H, C=C<u>H</u>–N) δ 7.51 (d, $J = 4.4$ Hz, 1H, Ar–<u>H</u>) δ 7.49 (d, $J = 7.8$ Hz, 1H, Ar–<u>H</u>) δ 7.44 (s, 1H, Ar–<u>H</u>) δ 7.40 (d, $J = 7.7$ Hz, 1H, Ar–<u>H</u>) δ 5.54 (s, 2H, N–C<u>H</u>$_2$) δ 4.98 (s, 2H, C<u>H</u>$_2$–OH) δ 4.52 (s, 2H, C<u>H</u>$_2$–O) δ 4.46 (s, 2H, C<u>H</u>$_2$–O) δ 2.44 (s, 3H, N–C–C<u>H</u>$_3$); ^{13}C NMR (125 MHz, chloroform-*d*) δ 152.85, 132.87, 130.47, 129.06, 126.41, 123.04, 68.43, 61.65, 59.65, 50.39, 19.04; ^{19}F NMR (470 MHz, chloroform-*d*) δ −58.88 (s); IR (cm^{-1}) ν: 3117.83, 2897.75, 2927.20, 2378.42, 2390.56, 1185.75, 1683.20, 1283.30, 1215.78; HRMS (*m*/*z*): calculated for $C_{19}H_{20}N_4O_3F_3$ $[M + H]^+$ 409.1488; found, 409.1490; HPLC purity-98%; $t_R = 12.09$ min.

4.2 Biological activity

4.2.1 Inhibition experiment of AChE. For evaluation of AChE activity of the derivatives, we followed a modified Ellman's method using AChE from Electrophorus electricus[27]. After adding 0.1 M phosphate buffer solution (pH-8, 120 μL) to every well, AChE enzyme (0.5 U mL^{-1}, 10 μL) along with different concentrations of test compounds (20 μL) were added and incubated at room temperature for 15 minutes. After incubation, reaction mixture comprising of 75 mM acetylthiocholine iodide and 10 mM 5,5′-dithiobis-2-nitrobenzoic acid (DTNB) were added to 96 well plate to generate yellow colouration due to 5-thio-2-nitro-benzoic acid. Absorbance was measured immediately after addition of the reaction mixture in a kinetic loop for 10 minutes at 412 nm at an interval of 1 minute using BioTek Synergy HTX Multimode Microplate reader. All the samples were assayed in triplicate and IC_{50} values were determined and expressed as mean ± SEM as generated from Graph Pad Prism 8.0 software.

4.2.2 Antioxidant assay. The antioxidant capacity of all the compounds in our series were measured using oxygen radical absorbance capacity fluorescein (ORAC-FL) method previously described by Fang Lei *et al.*[28] with some modifications. The total reaction mixture was kept to 200 μL and 75 mM phosphate buffer solution was used for every assay. In dark 96 well plate, 25 μL of sample (8 μM)/Trolox (8 μM)/buffer was added along with 150 nM fluorescein solution (150 μL) and incubated in dark at 37 °C for 30 minutes. Following this, free radical initiator,

12 mM AAPH (25 μL) was added and immediately after addition, fluorescence readings were taken at excitation 485 nm and emission at 535 nm in a kinetic loop for 15 minutes at 1 minute interval. All the samples were assayed in triplicate in BioTek Synergy HTX Multimode Microplate reader. The area under the fluorescence decay curve (AUC) was calculated for every sample and total antioxidant capacity of the compound was determined by substractingit's AUC from the AUC of the blank. ORAC-FL values are expressed as Trolox equivalents and ORAC-FL value of Trolox is taken as 1. The ORAC-FL values of three individual experiments were expressed as expressed as mean ± SEM as generated from Graph Pad Prism 8.0 software.

4.3 Metal chelation study

Metal chelation studies of the tested compounds were done using UV spectrophotometer (Agilent Technologies 500) within the wavelength range of 200 to 600 nm at 37 °C. Solutions of $FeCl_3$, $CuCl_2$, $ZnSO_4 \cdot H_2O$, $AlCl_3 \cdot 6H_2O$, KCl, NaCl, $CaSO_4$, $Mg(OH)_2 \cdot 6H_2O$ and compounds to be tested were prepared, such that the resulting solution comprised 100 μM each of ligand and metal and incubated at 37 °C for 30 min. For taking the spectra of the compounds alone, metal solution was replaced with Milli Q water.

For affinity study of **5i** towards Fe, all metals Fe^{3+}, Zn^{2+}, Cu^{2+}, Ca^{2+}, Mg^{2+}, Na^+ and K^+ were mixed, such that the reaction mixture contained equal concentration each including the ligand **5i** as 100 μM.

For stoichiometric studies, 100 μM solution of **5i** was taken in the cuvette and to it 20 μL aliquots of 1 mM $FeCl_3$ was added till the final concentration reached of metal reached 100 μM. The concentration of $FeCl_3$ ranged from 10–100 μM and the titration was done in 37 °C.

4.4 *In silico* study

4.4.1 Molecular docking. The computational analyses of the compounds were done on Red Hat 5.0 Linux platform with Intel core 4 quad processor and 16 GB of RAM. The crystal structure of AChE (PDB ID 4EY5) was imported into Maestro software (Schrodinger Release 2019-3). The water molecules were removed and hydrogen bonds were added to the protein structure to make it adapt to an environment of pH 7, using protein preparation wizard, a function of maestro. Protein prep wizard utility was used to optimize the position of heavy atoms. The prepared protein was docked against the pyridoxine based triazoles by using the extra precession mode.

4.4.2 ADME prediction by SwissADME. The SwissADME software was accessed from http://www.swissadme.ch. The cdx. format of the structure was imported and the list of SMILES was entered and by clicking on the option RUN, the predictive properties were generated.

4.4.3 Toxicity prediction using ProTox-II. The online tool ProTox-II is a free open access web tool and accessed from http://www.tox.charite.de/tox. The input was provided with an integrated PubMed search of pyridoxine and then structural changes were done as per required for generating **5i**. The results were automatically generated as shown in Section 2.6.3.

Conflicts of interest

There are no conflicts to declare.

Acknowledgements

Tiyas Pal and Saipriyanka Bhimaneni are thankful to Department of Pharmaceutical, Ministry of Chemicals and Fertilizers for providing financial assistance. Spectral study was carried out at Central Instrumental Facility NIPER-R. NIPER-R/Communication/123.

References

1 P. Christina, *World Alzheimer's Report 2018, Alzheimer's Dis. Int. world Alzheimer Rep.*, 2018, pp. 1–48.
2 A. Cavalli, M. L. Bolognesi, A. Minarini, M. Rosini, V. Tumiatti, M. Recanatini and C. Melchiorre, Multi-Target-Directed Ligands to Combat Neurodegenerative Diseases, *J. Med. Chem.*, 2008, **51**(7), 2326.
3 R. R. Ramsay, M. R. Popovic-Nikolic, K. Nikolic, E. Uliassi and M. L. Bolognesi, A Perspective on Multi-Target Drug Discovery and Design for Complex Diseases, *Clin. Transl. Med.*, 2018, **7**(3), 1–14.
4 P. Mecocci and M. C. Polidori, Antioxidant Clinical Trials in Mild Cognitive Impairment and Alzheimer's Disease, *Biochim. Biophys. Acta, Mol. Basis Dis.*, 2012, **1822**(5), 631–638.
5 M. A. Silva, A. S. Kiametis and W. Treptow, Donepezil Inhibits Acetylcholinesterase via Multiple Binding Modes at Room Temperature, *J. Chem. Inf. Model.*, 2020, DOI: 10.1021/acs.jcim.9b01073.
6 H. Tachallait, A. Bouyahya, A. Talha, Y. Bakri, N. Dakka, L. Demange, R. Benhida and K. Bougrin, Concise Synthesis and Antibacterial Evaluation of Novel 3-(1,4-Disubstituted-1,2,3-Triazolyl)Uridine Nucleosides, *Arch. Pharm.*, 2018, **351**(11), 1–11.
7 A. Aziz Ali, D. Gogoi, A. K. Chaliha, A. K. Buragohain, P. Trivedi, P. J. Saikia, P. S. Gehlot, A. Kumar, V. Chaturvedi and D. Sarma, Synthesis and Biological Evaluation of Novel 1,2,3-Triazole Derivatives as Anti-Tubercular Agents, *Bioorg. Med. Chem. Lett.*, 2017, **27**(16), 3698–3703.
8 M. Irfan, B. Aneja, U. Yadava, S. I. Khan, N. Manzoor, C. G. Daniliuc and M. Abid, Synthesis, QSAR and Anticandidal Evaluation of 1,2,3-Triazoles Derived from Naturally Bioactive Scaffolds, *Eur. J. Med. Chem.*, 2015, **93**, 246–254.
9 A. Rastegari, H. Nadri, M. Mahdavi, A. Moradi, S. Sara, N. Edraki, F. Homayouni and B. Larijani, Bioorganic Chemistry Design, Synthesis and Anti-Alzheimer's Activity of Novel 1,2,3-Triazole-Chromenone Carboxamide Derivatives, *Bioorg. Chem.*, 2019, **83**, 391–401.
10 L. Jalili-Baleh, H. Nadri, H. Forootanfar, A. Samzadeh-Kermani, T. T. Küçükkılınç, B. Ayazgok, M. Rahimifard, M. Baeeri, M. Doostmohammadi, L. Firoozpour, S. N. A. Bukhari, M. Abdollahi, M. R. Ganjali, S. Emami,

M. Khoobi and A. Foroumadi, Novel 3-Phenylcoumarin–Lipoic Acid Conjugates as Multi-Functional Agents for Potential Treatment of Alzheimer's Disease, *Bioorg. Chem.*, 2018, **79**, 223–234.

11 X. Yang, X. Qiang, Y. Li, L. Luo, R. Xu, Y. Zheng, Z. Cao, Z. Tan and Y. Deng, Pyridoxine-Resveratrol Hybrids Mannich Base Derivatives as Novel Dual Inhibitors of AChE and MAO-B with Antioxidant and Metal-Chelating Properties for the Treatment of Alzheimer's Disease, *Bioorg. Chem.*, 2017, **71**, 305–314.

12 M. Yazdani, N. Edraki, R. Badri, M. Khoshneviszadeh, A. Iraji and O. Firuzi, Multi-Target Inhibitors against Alzheimer Disease Derived from 3-Hydrazinyl 1,2,4-Triazine Scaffold Containing Pendant Phenoxy Methyl-1,2,3-Triazole: Design, Synthesis and Biological Evaluation, *Bioorg. Chem.*, 2019, **84**, 363–371.

13 Z. Najafi, M. Mahdavi, M. Saeedi, E. Karimpour-Razkenari, R. Asatouri, F. Vafadarnejad, F. H. Moghadam, M. Khanavi, M. Sharifzadeh and T. Akbarzadeh, Novel Tacrine-1,2,3-Triazole Hybrids: In vitro, In vivo Biological Evaluation and Docking Study of Cholinesterase Inhibitors, *Eur. J. Med. Chem.*, 2017, **125**, 1200–1212.

14 A. Kaur, S. S. Narang, A. Kaur, S. Mann, N. Priyadarshi, B. Goyal, N. K. Singhal and D. Goyal, Multifunctional Mono-Triazole Derivatives Inhibit $A\beta_{42}$ Aggregation and Cu^{2+}-Mediated $A\beta_{42}$ Aggregation and Protect against $A\beta_{42}$-Induced Cytotoxicity, *Chem. Res. Toxicol.*, 2019, **32**(9), 1824–1839.

15 M. R. Jones, E. L. Service, J. R. Thompson, M. C. P. Wang, I. J. Kimsey, A. S. Detoma, A. Ramamoorthy, M. H. Lim and T. Storr, Dual-Function Triazole-Pyridine Derivatives as Inhibitors of Metal-Induced Amyloid-β Aggregation, *Metallomics*, 2012, **4**(9), 910–920.

16 J. M. Zhuo and D. Praticò, Acceleration of Brain Amyloidosis in an Alzheimer's Disease Mouse Model by a Folate, Vitamin B6 and B12-Deficient Diet, *Exp. Gerontol.*, 2010, **45**(3), 195–201.

17 A. Hashim, L. Wanga, K. Junej, Y. Yeb, Y. Zhao and L. J. Ming, Vitamin B6s Inhibit Oxidative Stress Caused by Alzheimer's Disease-Related CuII-b-Amyloid Complexes-Cooperative Action of Phospho-Moiety, *Bioorg. Med. Chem. Lett.*, 2011, **21**(21), 6430–6432.

18 L. Drtinova, P. Dobes and M. Pohanka, Low Molecular Weight Precursor Applicable for Alzheimer Disease Drugs Synthesis (AChE and BChE Inhibition, BACE Inhibition, Antioxidant Properties and in Silico Modulation), *J. Appl. Biomed.*, 2014, **12**(4), 285–290.

19 A. Campbell, The Potential Role of Aluminium in Alzheimer's Disease, *Nephrol., Dial., Transplant.*, 2002, **17**, 17–20.

20 P. F. Good, D. P. Perl, L. M. Bierer and J. Schmeidler, Selective Accumulation of Aluminum and Iron in the Neurofibrillary Tangles of Alzheimer's Disease: A Laser Microprobe (LAMMA) Study, *Ann. Neurol.*, 1992, **31**(3), 286–292.

21 H. Akrami, B. F. Mirjalili, M. Khoobi, H. Nadri, A. Moradi, A. Sakhteman, S. Emami, A. Foroumadi and A. Shafiee, Indolinone-Based Acetylcholinesterase Inhibitors: Synthesis, Biological Activity and Molecular Modeling, *Eur. J. Med. Chem.*, 2014, **84**, 375–381.

22 G. Johnson and S. Moore, The Peripheral Anionic Site of Acetylcholinesterase: Structure, Functions and Potential Role in Rational Drug Design, *Curr. Pharm. Des.*, 2005, **12**(2), 217–225.

23 A. Daina and V. Zoete, A BOILED-Egg to Predict Gastrointestinal Absorption and Brain Penetration of Small Molecules, *ChemMedChem*, 2016, 1117–1121.

24 A. Daina, O. Michielin and V. Zoete, SwissADME: A Free Web Tool to Evaluate Pharmacokinetics, Drug-Likeness and Medicinal Chemistry Friendliness of Small Molecules, *Sci. Rep.*, 2017, **7**, 1–13.

25 M. N. Drwal, P. Banerjee, M. Dunkel, M. R. Wettig and R. Preissner, ProTox: A Web Server for the in Silico Prediction of Rodent Oral Toxicity, *Nucleic Acids Res.*, 2014, **42**, 3–8.

26 N. L. Morozowich, A. L. Weikel, J. L. Nichol, C. Chen, L. S. Nair, C. T. Laurencin and H. R. Allcock, Polyphosphazenes Containing Vitamin Substituents: Synthesis, Characterization, and Hydrolytic Sensitivity, *Macromolecules*, 2011, **44**(6), 1355–1364.

27 M. Pohanka, M. Hrabinova, K. Kuca and J. P. Simonato, Assessment of Acetylcholinesterase Activity Using Indoxylacetate and Comparison with the Standard Ellman's Method, *Int. J. Mol. Sci.*, 2011, **12**(4), 2631–2640.

28 K. Pérez-Cruz, M. Moncada-Basualto, J. Morales-Valenzuela, G. Barriga-González, P. Navarrete-Encina, L. Núñez-Vergara, J. A. Squella and C. Olea-Azar, Synthesis and Antioxidant Study of New Polyphenolic Hybrid-Coumarins, *Arabian J. Chem.*, 2018, **11**(4), 525–537.